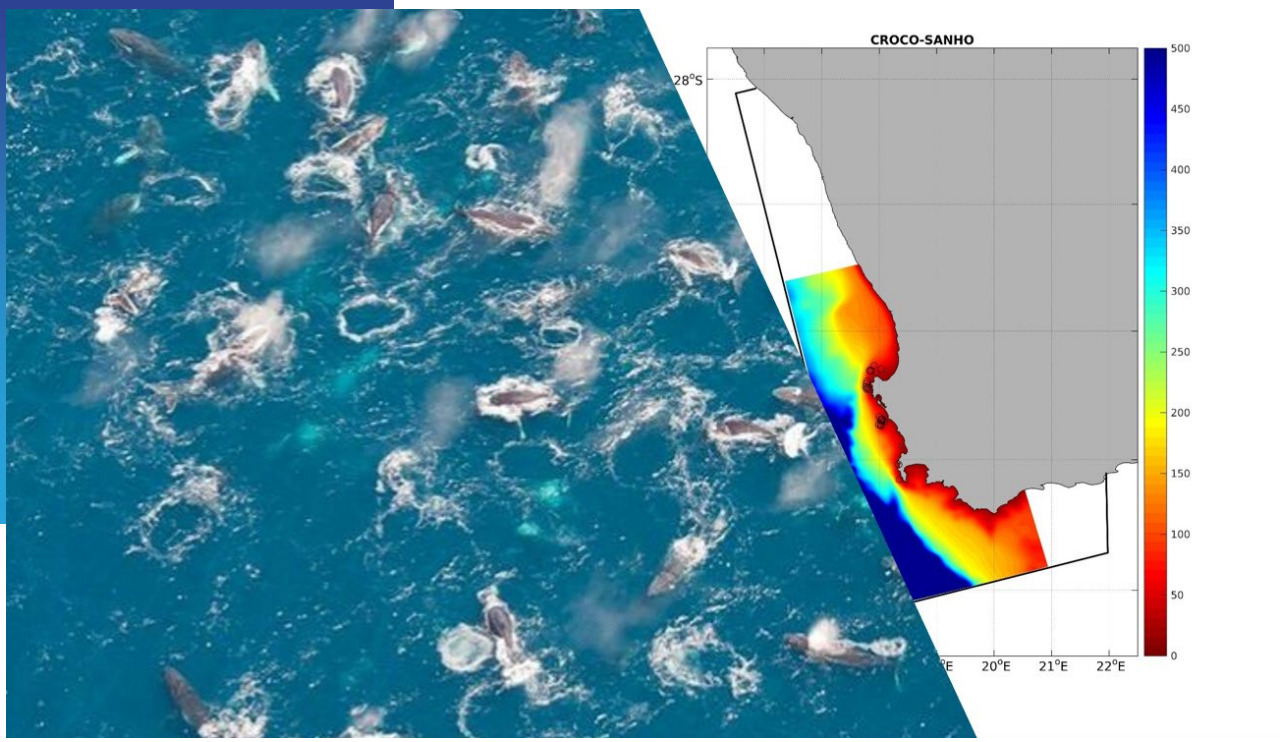

Implementation of a regional ocean model for the study of humpback whale super-groups in the southern Benguela

Subhra Prakash Dey and Marcello Vichi

Marine Research Institute,
University of Cape Town
South Africa

May 2020

Ma-Re
Marine Research Institute
Whales & Climate
Research Program

Executive Summary

This technical report illustrates the ocean numerical model that has been created to assist the research on super-group sightings in the South African West coast. Since 2011, large assemblages of humpback whales, called super-groups, have been observed in the Southern Benguela in spring. The ocean numerical model CROCO is being used to simulate the main oceanographic patterns and link the sightings to changes in the general circulation and other environmental conditions.

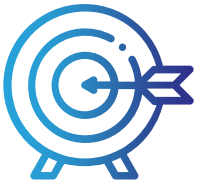

Rationale for the model implementation

A regional ocean model allows to describe the major oceanographic features in the Southern Benguela region, where humpback whales' super-groups have been observed since 2011.

Model Description

The model is based on the open-source CROCO system. It is currently forced with high-resolution atmospheric data for the period 2005-2012. The model is functional and ready to be run for longer periods.

Progress and preliminary results

Temperature and salinity biases at the open boundaries needs to be corrected to improve model simulations. Analysis of 18 years of chlorophyll-a data from 2001 to 2018 reveals greater-than-normal blooms about a month prior to the super-group events. Looking at the 2011 conditions in CROCO, these chlorophyll anomalies might be attributed to the reduced outward volume transport from the region.

Acknowledgments

The authors would like to acknowledge the contribution of Mr Giles Fearon who developed an earlier version of this model for his PhD thesis. This document is part of the international Whales & Climate project, managed by the Griffith University, in collaboration with Stellenbosch University and the Cape Peninsula University of Technology. We are grateful to the anonymous donor for the opportunity to carry out this research.
We would also like to acknowledge the Department of Environmental Affairs, Forestry & Fisheries for making the St Helena Bay monitoring line data available. We thank the DEFF Integrated Ecosystem Program for considering this project, and particularly Ashley Johnson and Keshnee Pillay.

Model Description

The chosen numerical ocean model for the Benguela simulation is the Coastal and Regional Ocean COmmunity model (CROCO, http://www.croco-ocean.org) CROCO is a three-dimensional terrain-following ocean model, which solves the primitive equations under the Boussinesq and hydrostatic approximations using finite difference numerical schemes (Shchepetkin and McWilliams, 2005; Deburu et al., 2012). This section describes the implementation of the larger scale model domain grid, which links the open ocean dynamics to the coastal processes where the whales are usually observed.

The model domain is presented in Fig. 1. The shape of the domain is constrained by the availability of atmospheric forcing, which is an essential feature to reproduce the topographic-driven upwelling conditions controlling the food availability in the region. The open black circles show the locations where the humpback whale super-groups were found (Findlay et al., 2017). The model domain has been designed to provide the necessary larger scale dynamics at the locations.

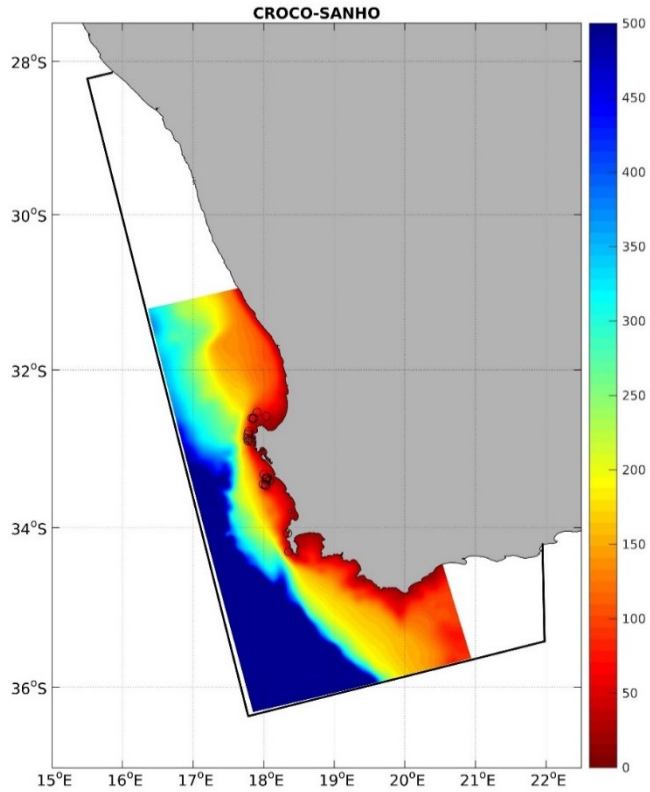

Figure 1 The model domain of the parent grid. Color shade shows the bathymetry used in the model. The domain enclosed by the black lines represent the region where the hourly atmospheric forcing data (WRF output) is available. The open black circles represent the locations where the humpback whale super-groups were found (data from table 1 of Findlay et al. 2017).

The bathymetry data were obtained from the hydrographic chart made by the South African Navy Hydrographic Office (SANHO) and then interpolated to the model grid using nearest neighbour interpolation. The model is forced at the surface by the atmospheric forcing available from the WRF model outputs developed by CSAG, University of Cape Town. The WRF outputs are rotated as shown in Fig. 1 (region bounded by the black lines). Our CROCO setup has 100 grid points in the zonal, 200 along the meridional direction and 50 vertical levels; and then the whole grid setup is rotated anticlockwise by 14.5° to make use of most of the available region covered by the atmospheric forcing dataset and reduce the number of grid points on land. This geometric setup allows us to represent the Agulhas current in the eastern boundary in a perpendicular way, and the Antarctic circumpolar current is tangential to the southern boundary of the model, which should lead to less numerical noise. The horizontal grid resolution of this domain is 3 km. CROCO allows to specify more vertical levels (sigma levels) towards the surface to resolve the surface layer processes better by adjusting the surface stretching parameter, θS (Song and Haidvogel, 1994). The same is done near the bottom by adjusting the bottom stretching parameter, θB. The θS and θB are set to be 7.0 and 2.0 for our simulation, respectively. Figure 2 shows the distribution of vertical sigma levels along 35°S. Table 1 shows the depths of all the 50 vertical levels where the minimum ocean depth is 20 m, and maximum is 3605 m.

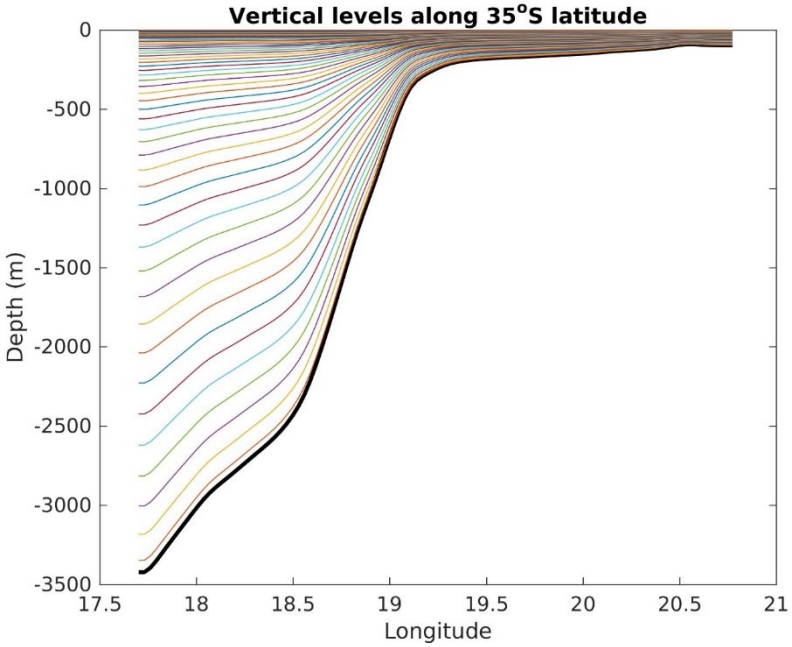

Figure 2: The vertical distribution of the sigma levels along the latitudinal section of 35o S.

The model is forced by the hourly high-resolution outputs of the atmospheric WRF model provided by CSAG, University of Cape Town. These outputs include specific humidity, surface pressure, precipitation, longwave and shortwave

radiation flux at the surface, sea surface temperature, surface air temperature (at 2 m height), zonal and meridional winds at 10 m height. All these variables are available at 3.3 km of spatial resolution. The momentum, heat, and freshwater fluxes are estimated in the model employing the bulk formulae described in Fairall et al. (1996). The initial and lateral boundary conditions are obtained from the HYCOM ocean reanalyses distributed by the Naval Oceanographic Office. The lateral boundary conditions include salinity, temperature, zonal and meridional currents, and surface elevation. All these datasets are available on a daily basis and spatial resolution of 9 km in 40 vertical levels. All variables are interpolated to the grid boundaries using linear interpolation.

Table 1. Depth of sigma levels at minimum depth, maximum depth and a point at continental slope

Vertical levels	Depth of the sigma levels at hmin (m)	Depth of the sigma levels over slope (m)	Depth of the sigma levels at hmax (m)	Vertical levels	Depth of the sigma levels at hmin (m)	Depth of the sigma levels over slope (m)	Depth of the sigma levels at hmax (m)
50	0	0	0	24	-9.589	-213.453	-350.81
49	-0.364	-3.668	-3.931	23	-9.973	-235.32	-393.053
48	-0.728	-7.472	-8.149	22	-10.36	-259.7	-440.586
47	-1.092	-11.415	-12.661	21	-10.75	-286.898	-494.052
46	-1.456	-15.505	-17.482	20	-11.144	-317.245	-554.144
45	-1.82	-19.752	-22.631	19	-11.541	-351.09	-621.603
44	-2.185	-24.166	-28.134	18	-11.943	-388.804	-697.206
43	-2.549	-28.765	-34.026	17	-12.35	-430.768	-781.755
42	-2.914	-33.568	-40.346	16	-12.761	-477.364	-876.054
41	-3.28	-38.597	-47.144	15	-13.179	-528.962	-980.886
40	-3.645	-43.881	-54.477	14	-13.602	-585.905	-1096.968
39	-4.011	-49.451	-62.413	13	-14.032	-648.481	-1224.907
38	-4.377	-55.345	-71.031	12	-14.468	-716.898	-1365.143
37	-4.744	-61.608	-80.424	11	-14.911	-791.248	-1517.869
36	-5.111	-68.288	-90.699	10	-15.361	-871.468	-1682.953
35	-5.479	-75.446	-101.976	9	-15.816	-957.299	-1859.847
34	-5.847	-83.147	-114.399	8	-16.278	-1048.237	-2047.491
33	-6.216	-91.469	-128.126	7	-16.744	-1143.494	-2244.229
32	-6.585	-100.498	-143.344	6	-17.214	-1241.969	-2447.741
31	-6.956	-110.334	-160.261	5	-17.686	-1342.233	-2655.019
30	-7.328	-121.092	-179.117	4	-18.158	-1442.543	-2862.393
29	-7.701	-132.899	-200.182	3	-18.628	-1540.895	-3065.646
28	-8.075	-145.9	-223.763	2	-19.093	-1635.122	-3260.215
27	-8.45	-160.261	-250.204	1	-19.551	-1723.039	-3441.501
26	-8.828	-176.166	-279.895	0	-20	-1802.63	-3605.259
25	-9.207	-193.82	-313.269				

Experimental set-up

We simulated the physical ocean state for the period 1 November 2005 to 31 December 2012, the period covered by the high-resolution atmospheric forcing obtained from CSAG. This period includes three super-group sightings in November 2011 (Findlay et al., 2017).

Figure 3 shows the time series of surface- and volume-averaged kinetic energy, volume averaged w, temperature, and salinity to understand whether the model has become stable. Analysing the mean kinetic energy, temperature, and salinity time series, we can say the model has reached a stable equilibrium after 2006.

CROCO performance and assessment

This section and the following present some details on model performances, evaluate the model biases and illustrate the necessary corrections to improve the ocean state description in the years before and during the sightings.

Figures 4 and 5 compare the seasonal climatology of CROCO simulated sea surface temperature (SST) and surface salinity with the HYCOM reanalysis product, which was used for lateral boundary conditions. The model captures the seasonal variation of SST impressively; however, an overestimation is found during summer and fall at the northern St. Helena bay. CROCO captures the surface salinity also very well. The low salinity at the north of Cape Columbine in the reanalysis data was not captured by the model.

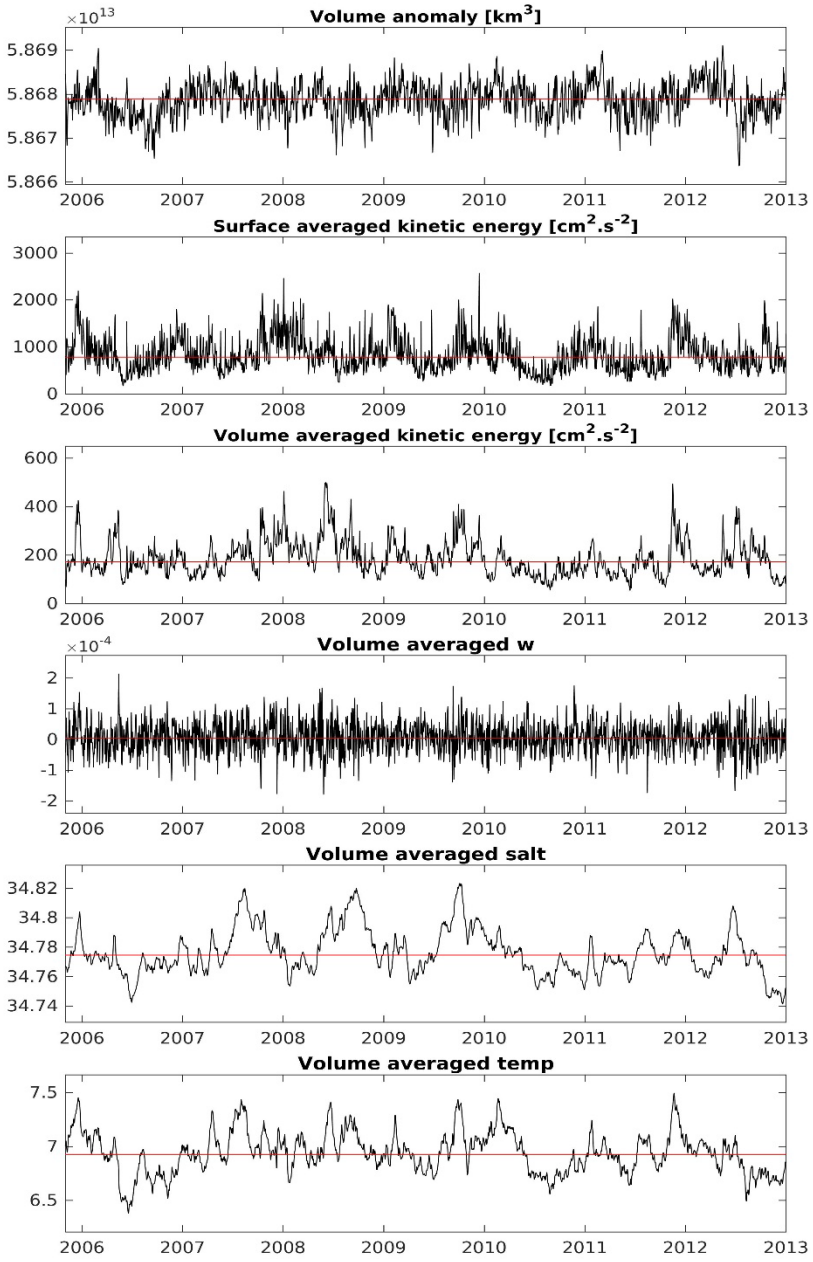

Figure 3: CROCO stability diagnosis. The panels from the top show the time evolution of volume anomaly, surface, and volume-averaged kinetic energy, volume averaged vertical velocity, salt, and temperature, respectively.

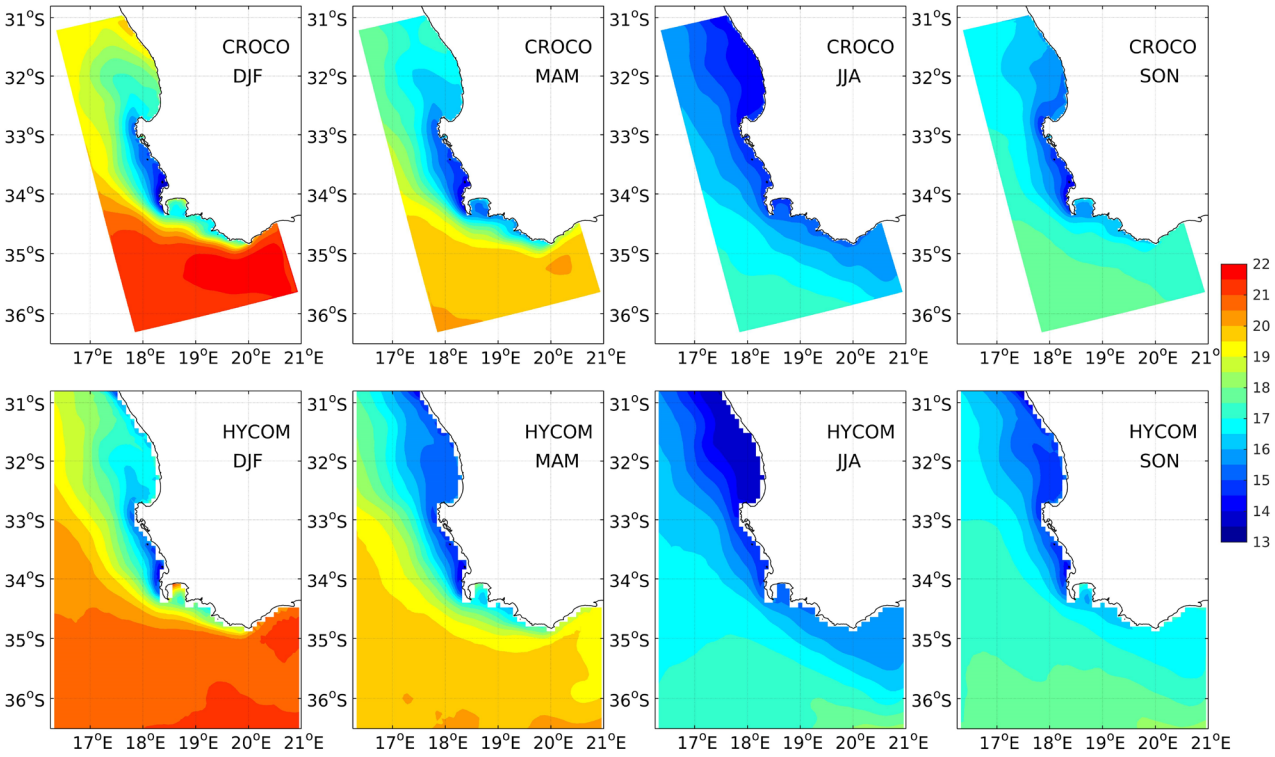

Figure 4: Comparison of seasonal sea surface temperature climatology of CROCO and HYCOM reanalysis (the boundary condition).

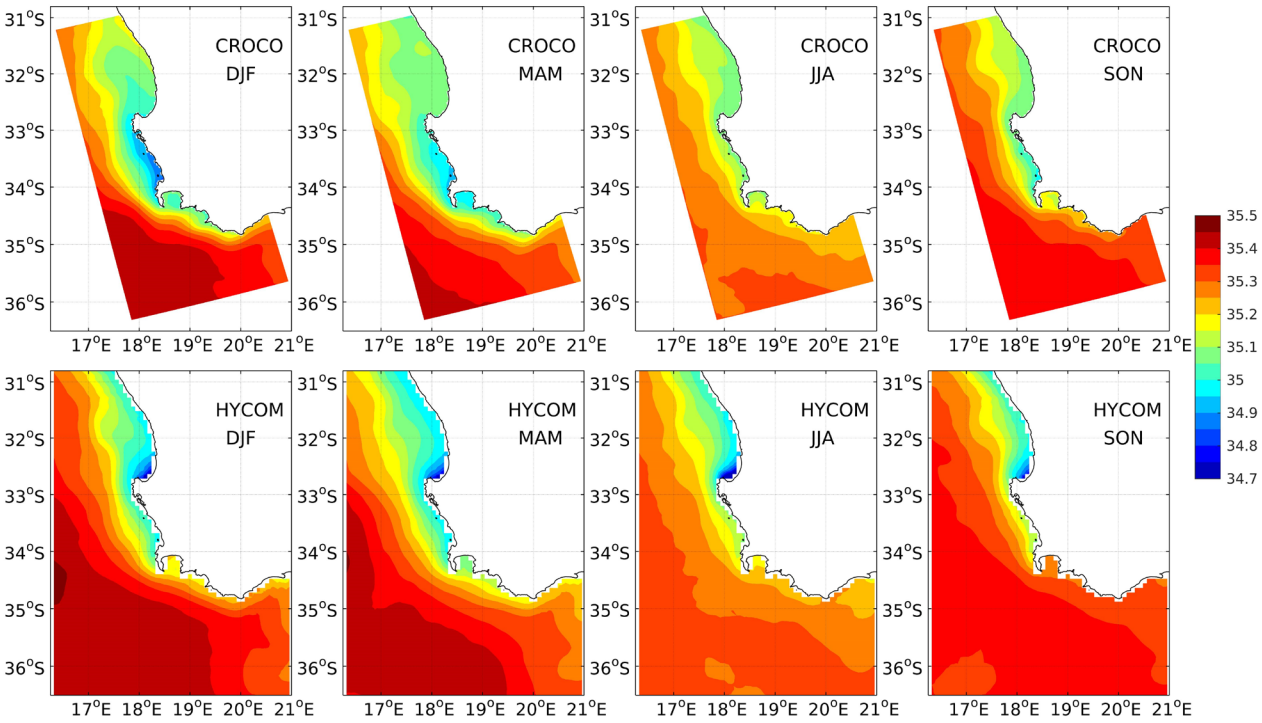

Figure 5: Comparison of seasonal surface salinity climatology of CROCO and HYCOM reanalysis (the boundary condition).

Figure 6 shows the differences in climatological seasonal averaged vertical section of temperature bias of CROCO estimated using the observations at nine monitoring stations along a line called St Helena Bay monitoring line (SHBML). These observations are cruise measurements performed by the Department of Environmental Affairs, Forestry & Fisheries. CROCO shows a warm bias of around 4°C at the subsurface particularly during December – February, and September – November. This might be due to improper intrusion of high-temperature water mass from the boundaries. To improve this bias we corrected the temperature and salinity at the open boundaries and re-run the model. The bias at the open boundaries is assumed to be the differences of climatological HYCOM salinity and temperature from CSIRO Atlas of Regional Sea 2009 (CARS 2009) climatology. The CARS climatology was derived from a

quality-controlled archive of all available historical subsurface ocean property measurements. Since the CARS climatology is available on a monthly basis, we estimated the monthly bias first and then linearly interpolated to make daily and corrected the daily updating HYCOM lateral boundary condition. The radiative open boundary schemes as proposed by Orlansky (1976) was adopted for this simulation. A weak nudging of relaxation time 360 days was specified for outward propagation inhibiting unwanted reflections while a strong nudging of a 1 day relaxation period was specified for inward propagation enabling strong adaptability with external data without causing over-specification problem following Marchesiello et al., 2000.

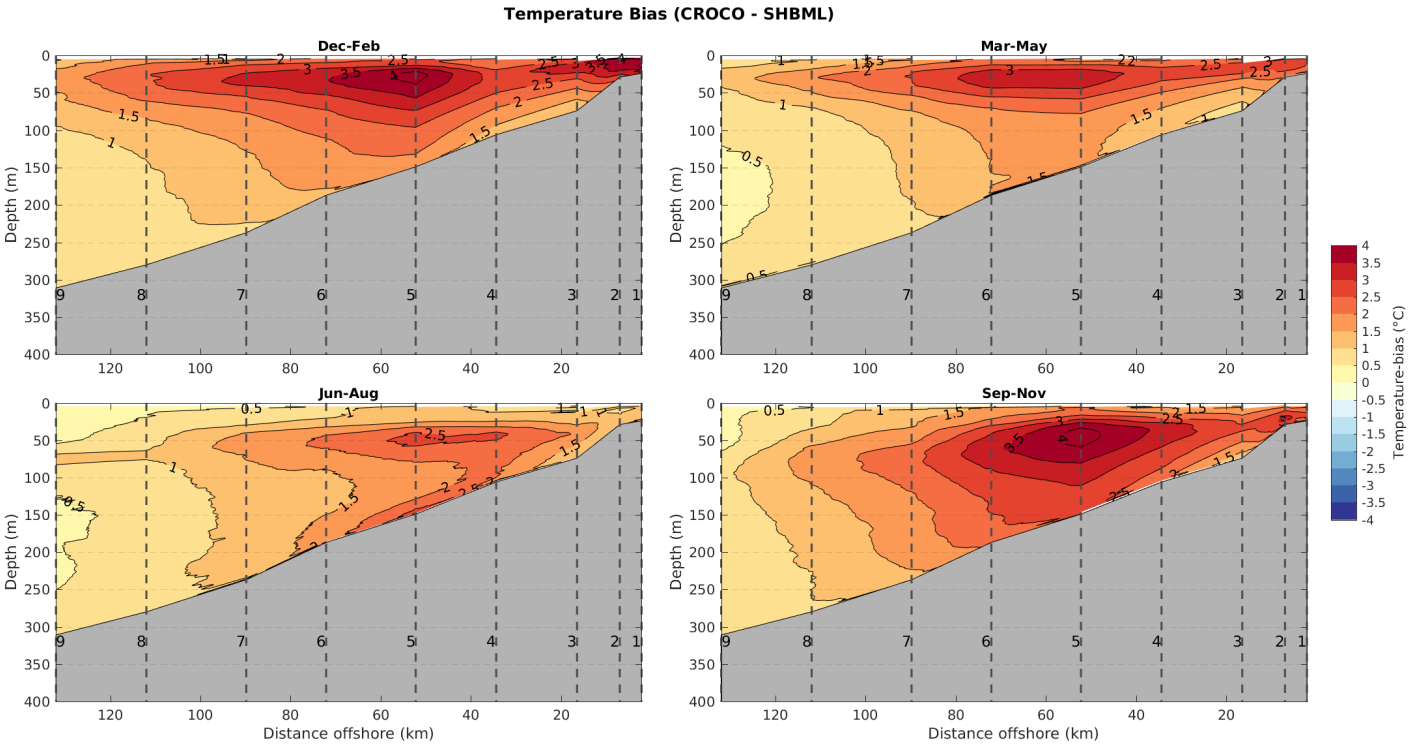

Figure 6: Vertical section of seasonal averaged temperature bias in CROCO simulation along the SHBML. The bias was calculated by subtracting the climatological SHBML measurement from the CROCO climatology. The vertical dashed lines associated with numbers 1 – 9 represent the positions of the monitoring stations.

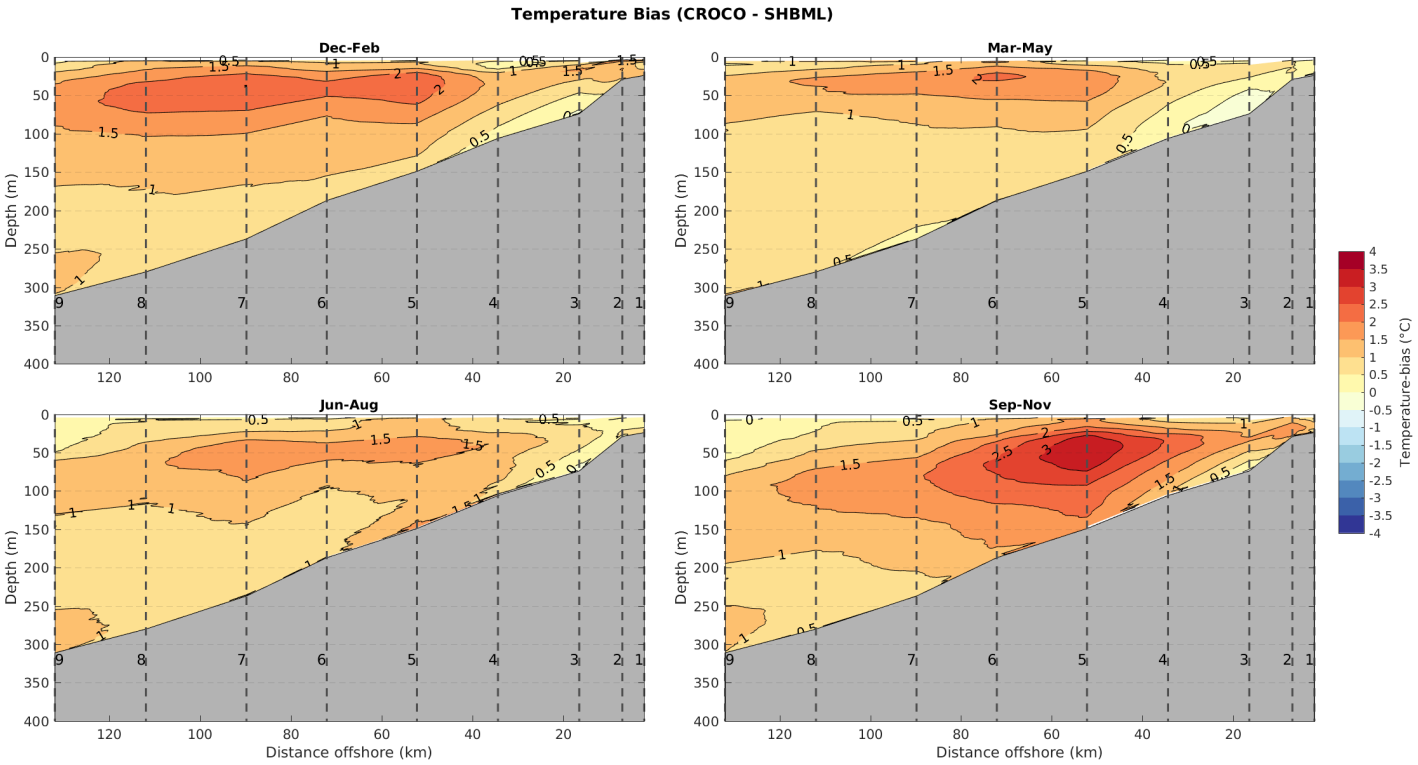

Figure 7: Similar vertical section of temperature bias as figure 6 but estimated from the CROCO simulation with corrected lateral boundary conditions.

Figure 7 shows the similar vertical sections of temperature bias of CROCO as shown in figure 6, but after correcting the boundary values of temperature and salinity as mentioned above. The bias reduces significantly in all seasons after this correction. However, a reduced warm bias of 3°C is noticed at the subsurface near station 5 in September – November.

Figure 8 compares the temperature and salinity profiles of uncorrected and boundary corrected or debiased CROCO simulations with ARGO floats at two locations on two randomly picked days, January 7, 2012, and May 23, 2009. Overall both the simulations capture the temperature and salinity profiles; however, debiased simulation replicates the observations better. The location of the ARGO float on January 7, 2012, was at 36°S, 18.5°E, which is very near

to the southern open boundary of the model setup. Both the simulations capture the profiles impressively and even better in the debiased simulation. The location of the ARGO float on May 23, 2009, was at 35.7°S, 18.1°E, comparatively far from the model open boundary. Some mismatches in the salinity profile are noticed here in both the simulations compared to the observation at the surface layer (top 200 m). However, the boundary corrected simulation captures the along-depth salinity variation up to a certain extent.

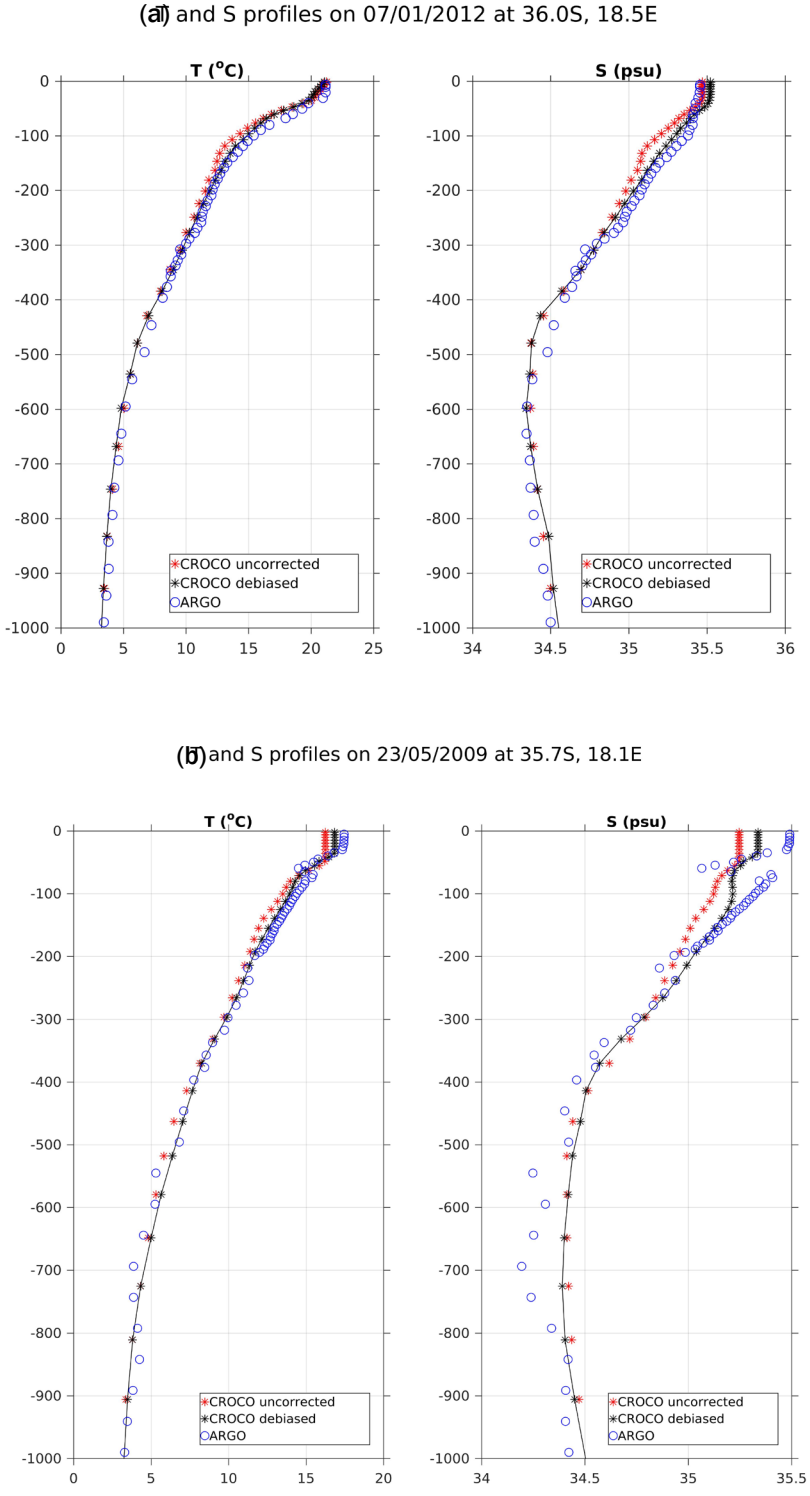

Figure 8: Comparison of temperature and salinity profiles of uncorrected and bias-corrected or debiased CROCO simulations with that of ARGO float at two locations at two different time: (a) at 36°S, 18.5°E on January 7, 2012, and (b) at 35.7°S, 18.1°E on May 23, 2009.

Chlorophyll from space and humpback super-groups

Findlay et al., 2017 reported that the super-groups were found showing feeding behaviour from the last week of October to mid-November in three years, 2011, 2014, and 2015. Figure 9 shows the year-wise comparison of chlorophyll anomaly obtained from the ESA ocean color CCI dataset and averaged for the period 15 October to 15 November, the period when super-groups were found. Analysing all these maps, an increase in primary production is evident when the super-groups were sighted. We chose the three boxes as shown in figure 9 covering the super-groups locations for a detailed analysis.

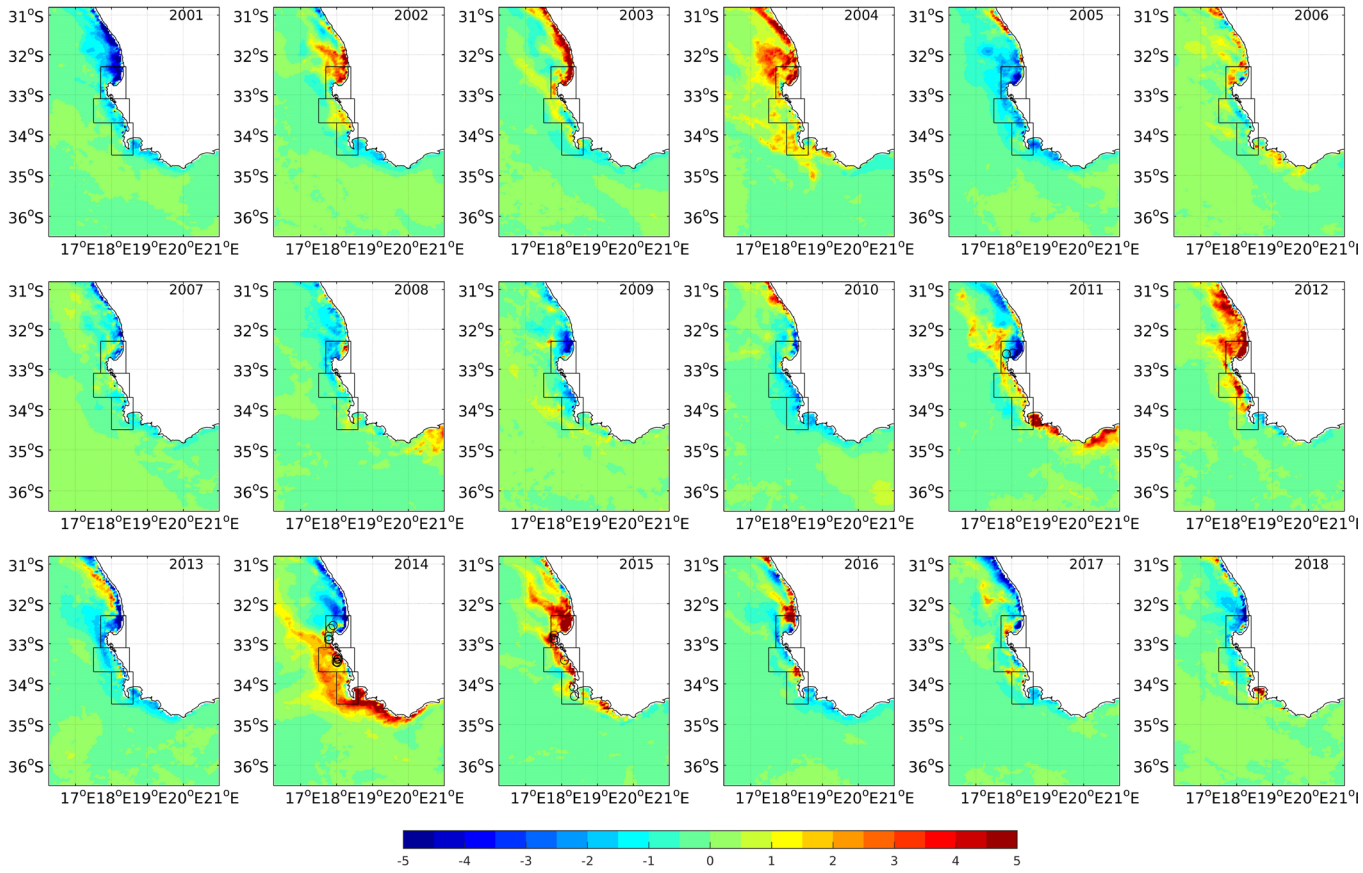

Figure 9: Chlorophyll-a anomaly averaged from 15 October to 15 November, the one-month period when the super-groups were sighted. The open circles show the locations where the

super-groups were observed. The tiny boxes covering the super-group locations are chosen for our analysis.

Figure 10 shows the time series of September – November primary production averaged in the mentioned three boxes and the occurrences of the super-groups. A chlorophyll bloom is always evident during/before the occurrence of the super-groups. The lag of supper-groups occurrence from the chlorophyll bloom could be due to the lag between the primary and secondary production, which is needed to be examined later.

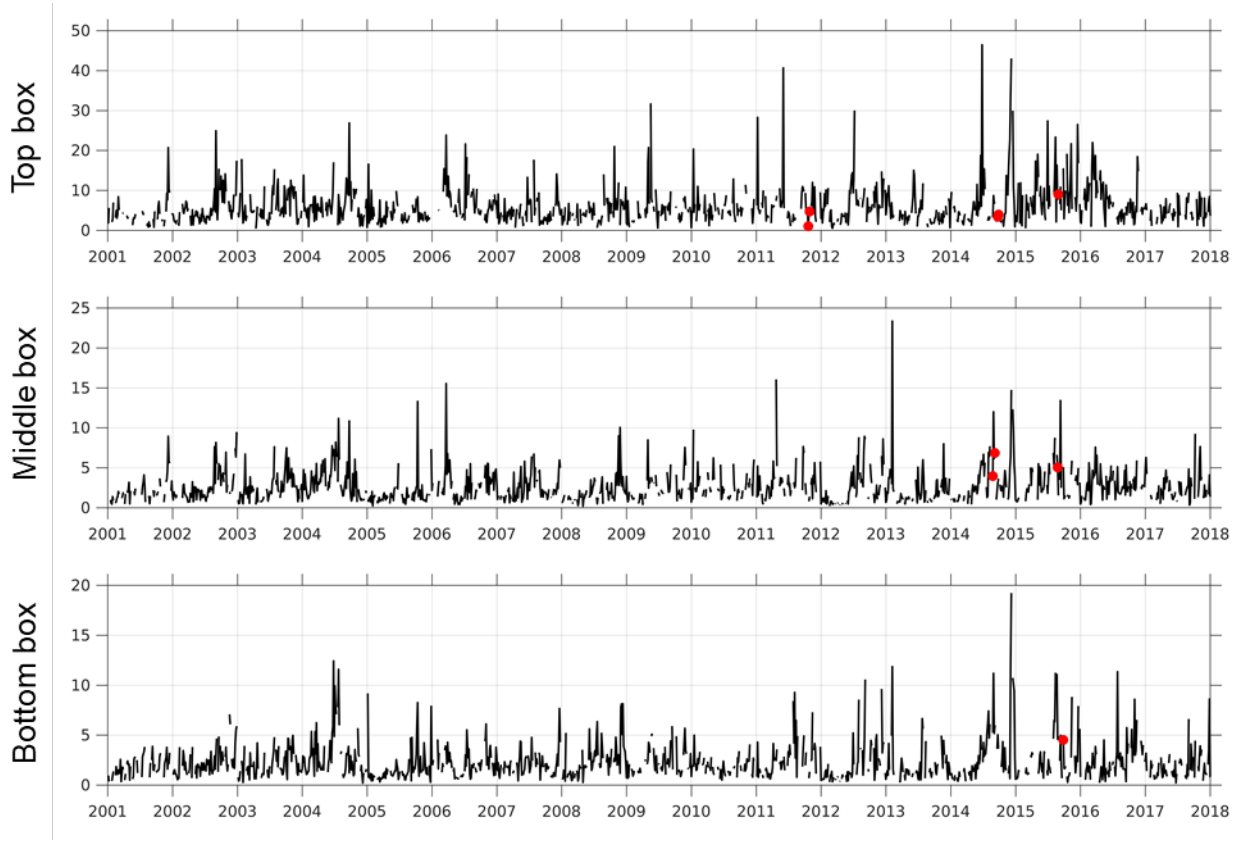

Figure 10. Daily chlorophyll-a averaged over the three boxes and the red dots show the occurrence of the super-groups. The chlorophyll-a of only September to November in each year is plotted.

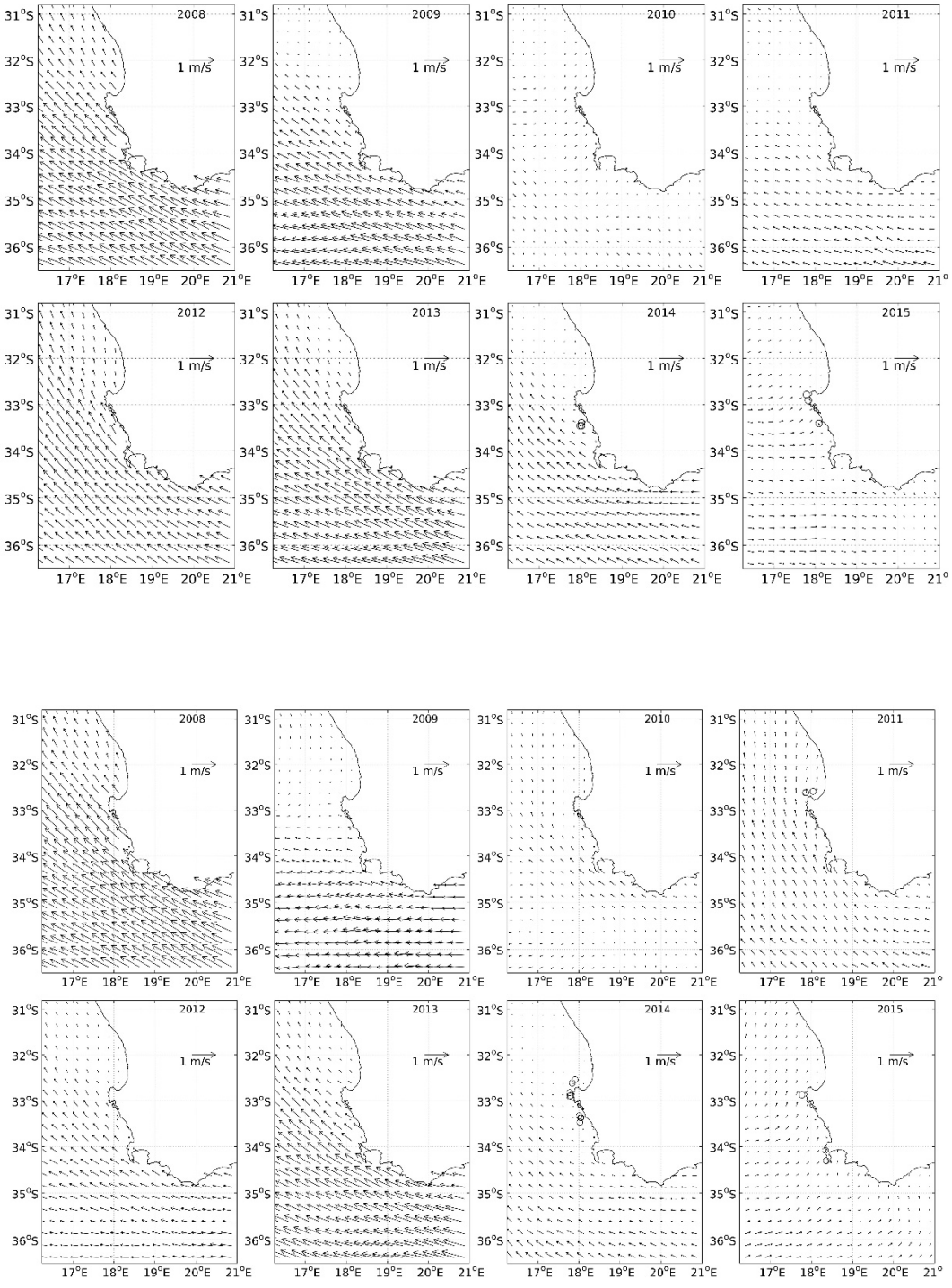

Figure 11. Comparison of wind stress in different years used to force CROCO averaged for October (top) and November (bottom). Data obtained from the ASCAT scatterometer.

Changes in the water transport

Chlorophyll blooms in the Benguela region are typically related to two physical processes: the wind-driven coastal upwelling and the surface circulation. These mechanisms can however be connected, in the sense that a change in upwelling conditions may lead to baroclinic anomalies which in turn would modify the current. A detailed inspection of wind stress conditions during the months of the sightings (Figure 11) excluded the more direct coastal upwelling factor. October and November 2011 were characterized by the lowest wind stress in the analysed period.

The changes in chlorophyll concentration should be highly correlated with retention in the region and therefore with the outward volume transport from the region. Hence the outward volume transport could be used as a proxy for biomass retention. The blue boxes in Figure 12 show the regions where we calculated the outward volume flux using CROCO output. These boxes also enclose the super-group sighting locations but rotated by the same sense as our grid for making the calculation easier. Furthermore, these boxes also enclose similar areas as the boxes where the chlorophyll concentration was averaged (see figure 12). The super-groups were found at the northern (or top) box on 12 – 14 November 2011. The preceding chlorophyll bloom at the top box found around in the second week of October (nearly one month before the super-groups occurrence). Figure 13 compares the outward volume transport through the western, southern and northern boundary of each box and for the whole region as shown in figure 12 averaged during 1 – 20 September (nearly one month before the chlorophyll bloom; this was decided by analysing the net

outward transport and chlorophyll time series together). The total outward transport is lowest in 2011 at the top box compared to all the other years.

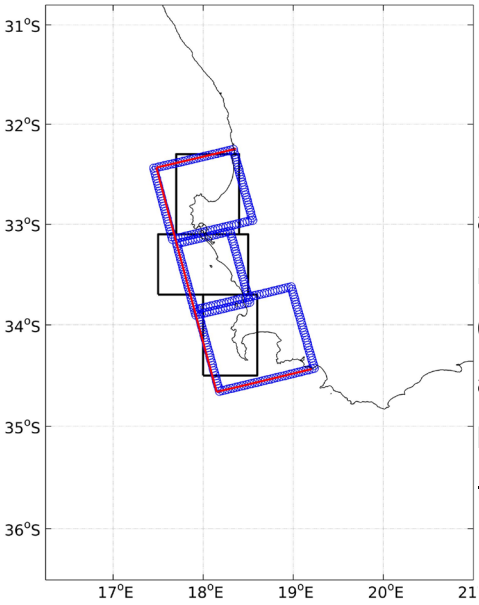

Figure 12: The black boxes show the region where we averaged chlorophyll-a. The blue boxes show the regions considered for the transport calculation from CROCO output. These boxes have the same rotation as our model grid. The region enclosed by the red lines was considered for calculating the total transport.

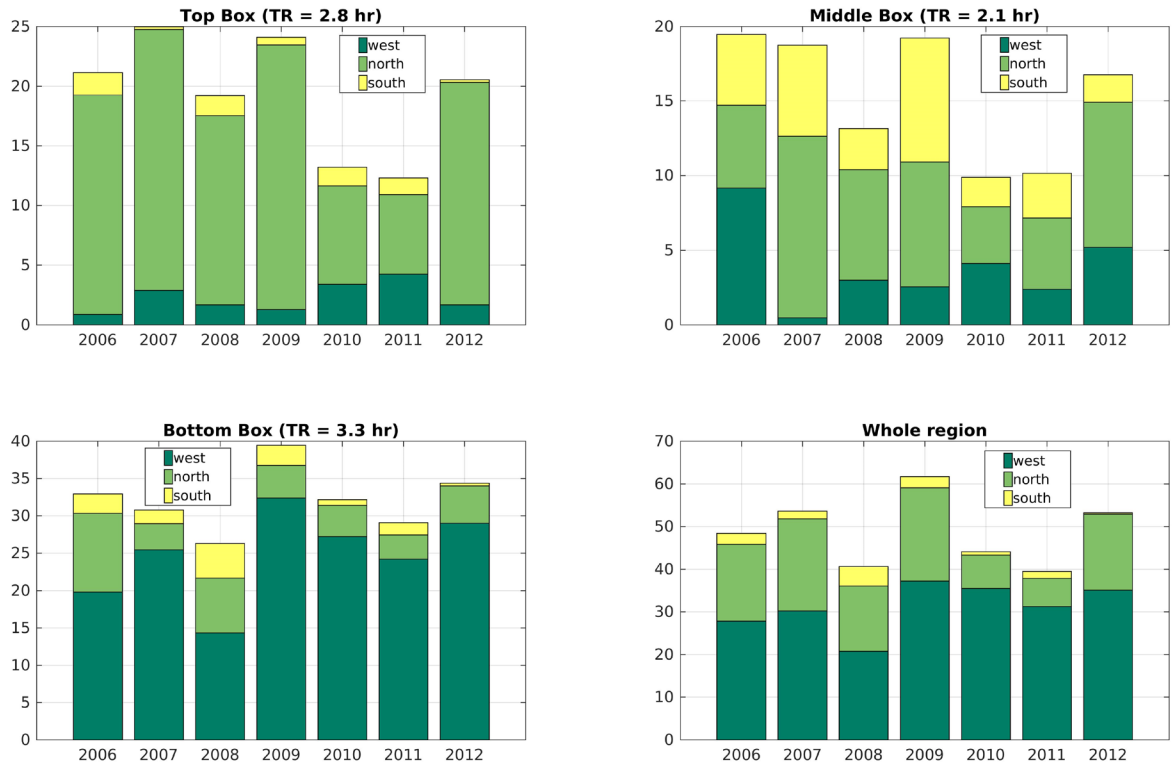

Figure 13: Outward volume transport (in Sv) calculated from CROCO output at the upper 100 m of water at all the three boxes and the whole region. The shading labelled west, north, and

south stand for the outward transport through the western, northern, and southern boundary. The residence time (TR) at each box was estimated considering the net outward transport through all the open faces of the boxes.

The northward transport which is attributed to the Benguela Jet is dominant in this box. The northward transport from this box is also weak during 1 – 20 September in 2010 and 2011 indicating a weakening of the Jet at that time. Though the westward transport in 2012 is the smallest compared to other years, the northward transport or the Jet was so intense it flushes out the primary production from the region. Interestingly enough, no super-group was sighted in 2012 which strengthen our hypothesis of lower primary production because of enhanced outward volume transport. If we consider the whole region or the total area of all the three boxes, the net outward transport from the area was the least in 2011.

The role of vertical stratification

Before making the above mentioned points it is also very important to check whether our CROCO setup simulates the transport properly. Unfortunately, no observation for subsurface currents is available in our study region for validating our modelled transports. However, we can assume that the currents will be dependent on density stratification. The density stratification can be validated with observations more easily. If our model captures the density stratification and its time variation properly, it is more likely to capture the related baroclinic ocean currents, which are characteristics of the Benguela jet region. The potential energy anomaly (PEA) can be considered as a proxy for density stratification. The PEA is defined as (Yamaguchi et al., 2019)

$$PEA = \frac{1}{H}\int_{-H}^{0}(\bar{\rho} - \rho)gz\,dz$$

Where ρ is the potential density and $\bar{\rho}$ is the vertically averaged potential density. PEA represents the amount of energy per unit volume that is required to make the density-stratified water column vertically homogeneous. Hence higher PEA represents strong density stratification. Figure 14 compares the PEA estimated from SHBML observation at station 8 with that estimated from uncorrected and bias-corrected CROCO simulations at the same location which brings out the necessity of correcting the open boundaries for improving the vertical stratification and hence the transport estimations.

Both the simulations show a high correlation with the observation and of course more similarities with observations in the bias-corrected simulation particularly during 2010 – 2011. Station 8 is located at deep ocean, nearly 115 km offshore from the coast. Figure 15 shows similar plots as figure 13 but at the location of station 2 which is located very near to the coastline. Both the simulations show similar variations indicating the reduced impact of open boundary conditions at this position.

Table 2 shows some performance indicators to assess the skill of the model in simulating/estimating the PEA, namely the mean, Root Mean Square Differences (RMSD), Bias (B), Average Absolute Error (AAE). The details of these indices were presented in Vichi and Masina (2009). Both the RMSDs (RMD_{TOT} and $RMSD_{CP}$), absolute bias, and AAE are found to be lower at both the stations after the bias correction at the open boundaries, indicating improvement in estimating PEA. However, more improvement is noted at station 8 which is near the open boundary of the model compared to station 2, a near-shore location station.

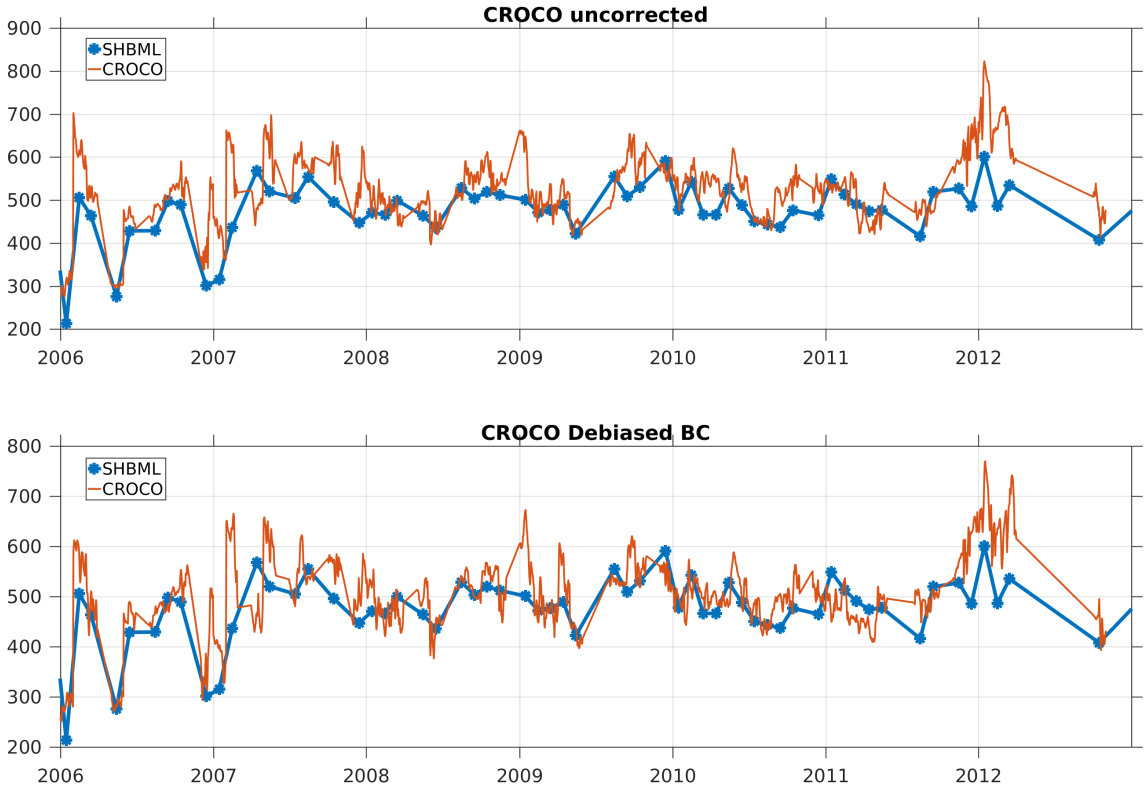

Figure 14: Comparison of PEA variation estimated from SHBML observation (Blue line) at station 8 with that estimated from uncorrected CROCO simulation (the orange line at the top panel) and boundary corrected CROCO simulation (the orange line at the top panel) at the same location.

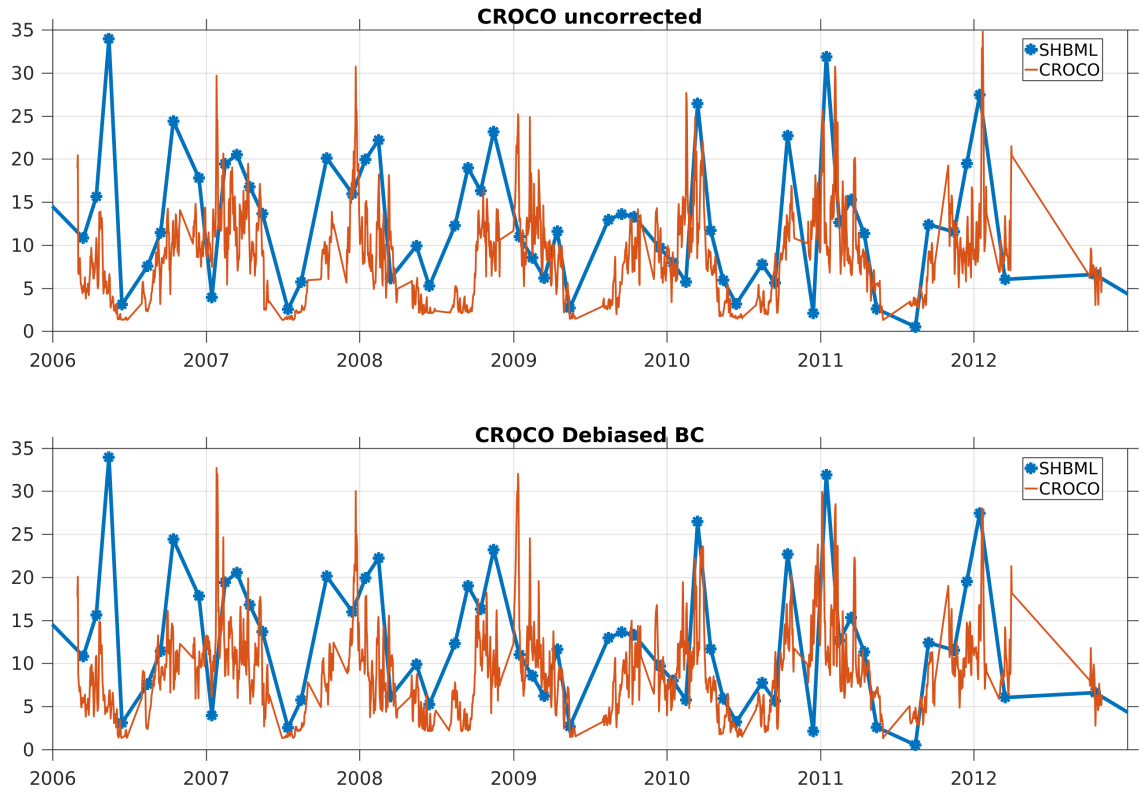

Figure 15: Similar plot as figure 13 but at station 2.

Table 2: Skill assessment indices of uncorrected and boundary corrected CROCO simulation in estimating PEA at two monitoring stations: stations 2 and 8.

Simulation	Stations	Mean	$RMSD_{TOT}$	$RMSD_{CP}$	B	AAE
Uncorrected CROCO	Station 2	8.4	7.6	6.3	-4.3	5.9
	Station 8	524.1	75.9	59.5	47.2	56.9
Debiased CROCO	Station 2	8.4	7.5	6.4	-4.0	5.8
	Station 8	524.1	64.1	57.9	27.5	46.7

Figures 13 and 14 and Table 2 suggest that our model is capable to capture the variation of density stratification and hence the volume transport. The picture becomes even clearer when salinity and temperature biases are corrected at the open boundaries. The reduced outward volume transport in the near-shore region as depicted in figures 9 and 10 on 1 – 20 September 2011 could retain excess primary production which produces plenty of secondary production followed by the super-group events around a month later. This hypothesis will be further explored by means of the biogeochemical CROCO simulation. Furthermore, a Lagrangian approach to study the transport and chlorophyll retention could help to better elucidate the process.

Future work

1. Our model simulation covers only one super-group event which was in 2011 which inhibits to draw any strong inference regarding super-groups. We need to run our simulation for a longer period. We may use a coarser atmospheric forcing such as CFSR to perform this unless the high-resolution forcing is available.
2. A biogeochemical module will be coupled with the CROCO to simulate the changes in feeding conditions for the whales and understand the process behind it.

References

Debreu, L., Marchesiello, P., Penven, P. and Cambon, G., 2012. Two-way nesting in split-explicit ocean models: algorithms, implementation and validation. Ocean Modelling, 49, pp.1-21.

Fairall, C.W., Bradley, E.F., Rogers, D.P., Edson, J.B. and Young, G.S., 1996. Bulk parameterization of air-sea fluxes for tropical ocean-global atmosphere coupled-ocean atmosphere response experiment. Journal of Geophysical Research: Oceans, 101(C2), pp.3747-3764.

Findlay, K.P., Seakamela, S.M., Meÿer, M.A., Kirkman, S.P., Barendse, J., Cade, D.E., Hurwitz, D., Kennedy, A.S., Kotze, P.G., McCue, S.A. and Thornton, M., 2017. Humpback whale "super-groups"–A novel low-latitude feeding behaviour of Southern Hemisphere humpback whales (Megaptera novaeangliae) in the Benguela Upwelling System. PloS one, 12(3), p.e0172002.

Marchesiello, P., McWilliams, J.C. and Shchepetkin, A., 2001. Open boundary conditions for long-term integration of regional oceanic models. Ocean modelling, 3(1-2), pp.1-20.

Orlanski, I., 1976. A simple boundary condition for unbounded hyperbolic flows. Journal of computational physics, 21(3), pp.251-269.

Shchepetkin, A.F. and McWilliams, J.C., 2005. The regional oceanic modeling system (ROMS): a split-explicit, free-surface, topography-following-coordinate oceanic model. Ocean modelling, 9(4), pp.347-404.

Song, Y. and Haidvogel, D., 1994. A semi-implicit ocean circulation model using a generalized topography-following coordinate system. Journal of Computational Physics, 115(1), pp.228-244.

Yamaguchi, R., Suga, T., Richards, K.J. and Qiu, B., 2019. Diagnosing the development of seasonal stratification using the potential energy anomaly in the North Pacific. Climate Dynamics, 53(7-8), pp.4667-4681.

Vichi, M. and Masina, S., 2009. Skill assessment of the PELAGOS global ocean biogeochemistry model over the period 1980–2000. Biogeosciences.